Automatic Identification of Brain Contours in Magnetic Resonance Images of the Head

Fernando Bello* and Richard I Kitney

Biomedical Systems Group, Electrical Engineering Department,
Imperial College of Science, Technology and Medicine
London SW7 2BT
e-mail: f.bello@ic.ac.uk

Abstract— We present an automated procedure that can identify the contours of the brain from single-echo 3-D magnetic resonance (MR) images of the head. A first approximation to the desired contours is obtained by combining anatomical and MR imaging characteristics of the brain. A priori knowledge about the brain and its surrounding structures is then used to refine the original contours. This procedure has been successfully applied to various data sets from control patients, and a number of potential clinical applications are currently being considered.

1 Introduction

One of the present challenges in medical image processing is the segmentation of MR imaging data. Automated and semi-automated MR brain segmentation is relevant because of the large amount of data generated, and the need for reproducible brain analysis tools. A wide range of approaches has been proposed for the detection of various structures in the head [1-3].

In this paper we contribute a segmentation technique operating on single-echo 3-D MR images of the head. Being able to isolate the brain not only has the great advantage of reducing the amount of data to consider, but it is also a fundamental step to be carried out before any further classification or characterisation of brain tissues, in order to reduce computation time and complexity. Previous approaches include the use of different levels of histogram thresholding and morphological operations [5], a radial transform consisting of intensity profile analysis and the application of a series of heuristics [6], and a combination of 3D filters with watershed analysis [4]. The present approach is conceptually similar to that presented in [5], but it involves only one thresholding step and a smaller set of operations.

Our approach can be divided into three functional stages: Contrast Map generation, Contour Mask formation and Contour Mask refinement. These will be described in detail in the remainder of this paper.

---

* Sponsored by the Mexican National Research Council (CONACYT)

2 MR Data Sets

Our brain contour identification procedure was developed as a preliminary step for further identification of brain tissues and for clinical applications such as volumetric measurements of the brain. The data sets used for these test runs were acquired using a single echo pulse sequence on a 1.5T General Electric Signa scanner. They consist of 124 T_1-weighted coronal slices of dimension 256x256. Field of view was 240 mm minimised to encompass the head. Slice thickness was 1.5 mm and no inter-slice gap was used.

3 Contrast Map

In a MR image of the brain, the ring of high intensity seen around the boundary of the head corresponds mainly to adipose tissue (Fig. 1.(a)). By looking at horizontal profiles such as that of Fig. 1.(b), it can be seen that the adipose tissue is represented by the two largest peaks located on both sides of the profile. The width of such peaks is directly proportional to the amount of adipose tissue present. Due to the shape of the head, these peaks appear as high contrast pulse edges on a nearly semicircular fashion.

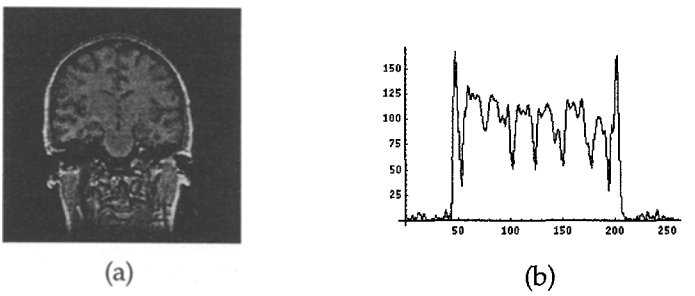

Fig. 1 (a) Brain MR mid-coronal slice and (b) horizontal profile at indicated location.

Based on the magnitude, width and location characteristics of these edges, it should be possible to apply a suitable edge detector to automatically map out these high contrast points of interest. Such an edge detector should be rotationally invariant to take into account the different orientations of the edges and have a response proportional to the edge contrast. It should also be possible to tune the detector to be sensitive to pulse edges of the desired width.

The Laplacian-of-Gaussian or LoG operator first proposed in [8] has these characteristics. It has been widely used in medical image analysis applications [3,4]. Although it tends to dislocate edges not complying with certain characteristics [9], we don't need to worry about this, as we are only interested in locating pulse-type edges of a certain width. Moreover, our concern is not the usual zero crossings detection, but analysing the actual values of the filtered image to extract the desired contrast information.

Consider the intensity profile of an ideal pulse edge of width $d = b - a$ such as that of Fig. 2.(a), and a LoG operator of size $M = 3w$, where w is the width of the excitatory region of the operator. The expected response obtained by performing the 1-D convolution of Eq. 1 and 2 is presented in Eq. 3 and graphically shown in Fig. 2.(b) for the case when $w \le d < M$. It has been shown [9] that for this case the resulting zero crossings will represent accurately the position of pulse edges.

$$\nabla^2 G(x) = \left(1 - \frac{x^2}{\sigma^2}\right) \exp\left(-\frac{x^2}{2\sigma^2}\right) \quad (1) \qquad I(x) = \begin{cases} 0 & \text{if } x > b, x < a \\ h & \text{if } a \le x \le b \end{cases} \quad (2)$$

$$C(x) = h \cdot \left. \frac{\alpha - x}{\exp\left(\frac{(x-\alpha)^2}{2\sigma^2}\right)} \right|_a^b = h \cdot \left(\frac{b - x}{\exp\left(\frac{(x-b)^2}{2\sigma^2}\right)} - \frac{a - x}{\exp\left(\frac{(x-a)^2}{2\sigma^2}\right)} \right) \quad (3)$$

As seen in Eq. 3, the magnitude of the peaks in Fig. 2.(b) is directly proportional to the edge contrast h. To detect pulse edges of the desired width d, we select a value for the scale constant σ large enough to guarantee only one positive peak at the mid-point of the pulse edge, but not so large as to dislocate the zero crossings from their expected positions. In other words, the magnitude of $C(x)$ at points a and b should be as close to zero as possible, and at point $d/2$ should have the largest possible magnitude. From our experiments, we know that d lies in the range of 10-15 pixels. Considering the minimum value of $d = 10$ and plotting the magnitude of $C(x)$ at the expected zero crossing locations of $x = a$ and $x = b$ (Fig. 2.(c)), and at the pulse mid-point of $x = d/2$ (Fig. 2.(d)), we see that a value of $\sigma = 3$ represents a good compromise. This value of σ is the one used in the present paper, where the separable property of the LoG operator has been exploited as in [10] to implement the LoG filtering operation with considerable computational savings.

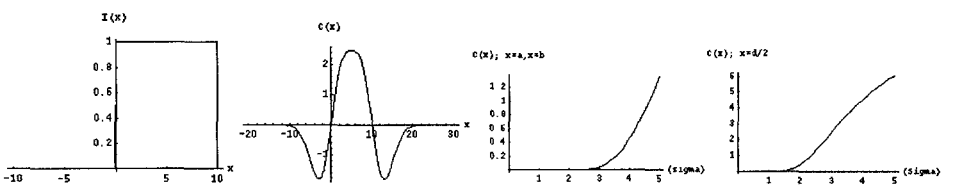

Fig. 2 (a) Edge profile with $a = 0$, $b = 10$, $h = 1$, (b) Response of a LoG operator with $w \le d$, $M > d$, and Magnitude of $C(x)$ at (c) expected zero crossing locations and(d) pulse edge mid-point.

By considering only the largest positive and negative peaks we concentrate on pulse edges having maximum contrast. Using the characteristic that pulse edges of interest will be located in a nearly semicircular fashion around the brain, and the fact that most of the brain is contained in the top half of a typical coronal slice, we can effectively generate a Contrast Map containing only those high contrast points of interest. An example of an absolute value LoG filtered image and its corresponding Contrast Map is illustrated in Fig. 3.(a) and (b).

4 Contour Mask

A Contrast Map shows locations in the original image where there are pulse edges of high contrast having a certain spatial configuration with respect to the brain. The expected positive peaks from the adipose tissue surrounding the brain almost form a closed path. It is not the same situation for the negative peaks that should indicate the skin/skull boundary (Fig. 3.(b)). Because these contours are not closed, they can not be directly used to identify the brain boundaries. Hence, two tracking/closing algorithms have been designed to obtain a binary Contour Mask that can be used to isolate the brain from the rest of the image.

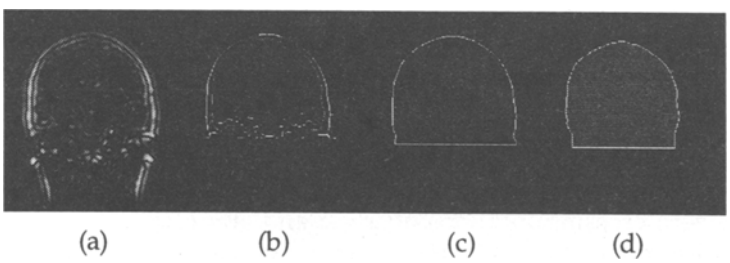

Fig. 3 (a) Absolute value LoG filtered image, (b) resulting Contrast Map, (c) Positive peaks Contour Mask and (d) negative peaks Contour Mask.

The first algorithm closes the positive and internal negative peaks paths for the top half. This procedure is repeated for the negative peaks, constraining its path to follow the same direction as the closed positive path, whenever a connection can not be made using a set of pre-defined templates.

The second algorithm approximates the brain contour for the bottom half. In this case there is no simple anatomical information to aid the tracking procedure. Therefore we make sure that no part of the brain is left out by finding its lowest point and using this as a landmark for the algorithm. An estimate for this lowest point is found by applying a peak differencing method to locate large bright to dark transitions in a number of equidistant vertical intensity profiles of the bottom half. An average location is obtained from transitions larger than a previously determined threshold, and it is used as the desired estimate. Fig. 3.(c) and (d) show the resulting Contour Masks for the positive and internal negative peaks of the Contrast Map in Fig. 3.(b).

5 Contour Mask Refinement

The brain is predominantly located in the superior portion of the head. By analysing the histogram of Fig. 4.(a) we can determine suitable thresholds for pixels located within the grey and white matter distributions. These thresholds are automatically obtained by using a parametric least squares (LS) fit of a sum of two Gaussians [11]. A bounded grey-value range limited on either side by the grey-value distance at one standard deviation from each peak is used to perform the fit. Upper and lower thresholds are calculated at two standard deviations away from each estimated mean. An example of the resulting LS curve fit is shown on Fig. 4.(b).

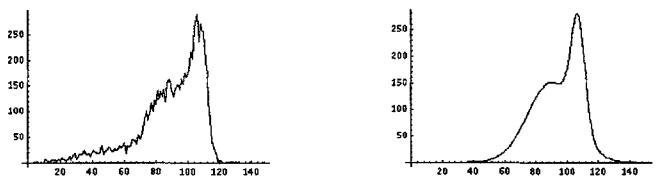

Fig. 4 (a) Grey-value histogram of top half obtained using negative peaks Contour Mask and (b) LS fit of sum of two Gaussians.

This thresholding procedure results in binary threshold masks including mostly brain pixels, but also pixels from other structures. Moreover, low-intensity pixels in the brain appear as holes in the threshold masks (Fig. 5.(a)). Morphological operations that allow us to match information from the shape and location of the different structures, with knowledge about anatomy and the imaging process are used to solve these problems. Finally, the brain is isolated from the remaining structures by selecting the region with the largest area. The result of applying this procedure to the binary threshold mask of Fig. 5.(a) is shown in Fig. 5.(b). Fig. 5.(c) presents the extracted brain.

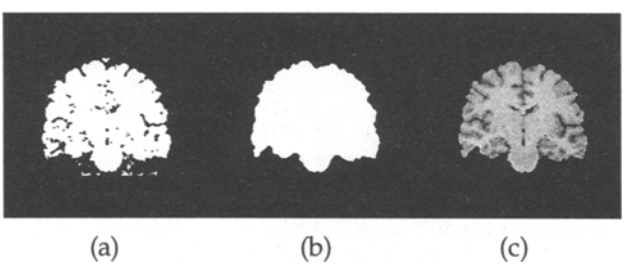

Fig. 5 (a) Binary threshold mask, (b) refined Contour Mask and (c) extracted brain.

6 Results and discussion

A total of 4 data sets were used for testing the identification procedure. Fig. 6 shows the final result for various slices of the different data sets.

Overall, the results of these test runs are encouraging and similar to those previously reported by other authors [4-6]. The procedure was successful in 80% of the slices. Most problems occurred in anterior and posterior slices, and in slices with large regions of visible bone marrow. Further improvements contemplated include using the third dimension by propagating the brain contours obtained from the middle slices, the use of a fixed distance to obtain the Contour Mask from the positive peaks contour in order to discard large bone marrow regions, and a region combination strategy that considers additional information to select brain regions from the labelled image

The procedure presented has been successfully used as a pre-segmentation step in a MR brain segmentation system [7]. Among the clinical applications being considered to further evaluate our approach are the measurement of total brain mass and measurement of total intracranial volume. Both of these measurements can be directly obtained from the Contour Masks presented in this paper.

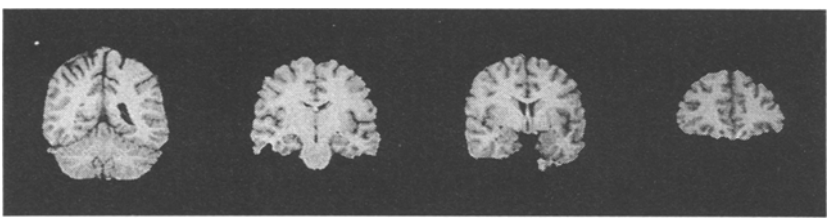

Fig. 6 Final contours of the brain obtained for various slices of the different data sets.

References

[1] **Kapouleas I**, *Segmentation and Feature Extraction for Magnetic Resonance Brain Image Analysis*, Proc. of 10th Intl. Conf. on Pattern Recognition, Atlantic City, 1:583, 1990.

[2] **Raya S**, *Low-level Segmentation of 3-D Magnetic Resonance Brain Images—A Rule-Based System*, IEEE Transactions on Medical Imaging 9:3, 1990.

[3] **Ehricke H**, *Problems and Approaches for Tissue Segmentation in 3D-MR Imaging*, Proc. SPIE Med. Imaging IV, 1233:128, 1990.

[4] **Katz W**, *et al*, *Segmentation of the Brain from 3-D Magnetic Resonance Images of the Head*, Proc. of 14th Annual Inter. Conf. of the IEEE EMBS, Paris, 1992.

[5] **Brummer M E** *et al*, *Automatic Detection of Brain Contours in MRI Data Sets*, IEEE Transactions on Medical Imaging 12:153, 1993.

[6] **Zijdenbos A P** *et al*, *Automatic Extraction of the Intracranial Cavity on Transvers MR Brain Images*, Proc. 11th Intl. Conf. on Pattern Recognition, The Hague, 3:430, 1992.

[7] **Bello F** and **Kitney R I**, *The Use of Regional Features to Segment Brain MRI*, Proc. IFMBE World Congress on Medical Physics and Biomedical Engineering, Rio de Janeiro, 1994.

[8] **Marr D** and **Hildreth E C**, *Theory of Edge Detection*, Proc. Royal Soc. London 207:187, 1980.

[9] **Huertas A** and **Medioni G**, *Detection of Intensity Changes with Subpixel Accuracy Using Laplacian—Gaussian Masks*, IEEE Transactions on Pattern Analysis and Machine Intelligence 8:651, 1986.

[10] **Sotak G E** and **Boyer K L**, *The Laplacian-of-Gaussian Kernel: A Formal Analysis and Design Procedure for Fast, Accurate Convolution and Full Frame Output* , Comput. Vision, Graphics and Image Processing 48:147, 1989.

[11] **Press W H** *et al*, *Numerical Recipes in C*, 2nd Ed., Cambridge University Press, Cambridge UK, 1991.